Real-time Estimation of Two-Dimensional Temperature Distribution in Lithium-ion Pouch Cells

Sara Sattarzadeh, Student Member, IEEE, Tanushree Roy, Student Member, IEEE, and Satadru Dey, Senior Member, IEEE

Abstract—Thermal management is an integral part of battery management systems due to the effect of temperature on safety, life-time and efficiency of batteries. Therefore, a reliable realtime estimation algorithm is required to estimate the temperature distribution in battery cells based on available measurements. Temperature estimation in pouch type cells is especially challenging due to the non-uniform distribution along length and breadth. Motivated by this issue, we study effective sensor placement and estimation algorithm design for pouch cells in this paper. Specifically, we explore two scenarios: Scenario 1 where multiple temperature sensors are available, and Scenario 2 where only one temperature sensor is available. For Scenario 1, we find the minimum number of sensors required and their effective locations whereas for Scenario 2 we find the effective location of the single sensor which maximize the state observability. We employ the Gramian observability analysis for this study. Subsequently, we design sliding mode observer based real-time algorithms for distributed temperature estimation in both scenarios. Finally, we illustrate the performance of the proposed estimation algorithms through extensive experimental and simulation studies.

Index Terms—Pouch cell, Observability, Sensor placement, Distributed thermal-model, Estimation.

I. INTRODUCTION

Pouch-type Lithium-ion battery cells have shown significant promise for electric vehicle applications [1]. From thermal behavior viewpoint, pouch cells exhibit additional complexities compared to cylindrical battery cells. For example, temperature distribution in cylindrical cells can be reduced to one dimension (in radial direction) assuming uniform distribution along the length [2]. On the other hand, pouch cells manifest significant temperature variation in at least two dimensions (along length and breadth) making such aforementioned assumption impractical. As temperature plays significant role in safety, capacity fade, and impedance rise, it is critical to monitor cell temperature distribution in real-time operation [3], [4].

Thermal models of pouch cells can be categorized into lumped, two dimensional (2D), and three dimensional (3D) models. Lumped models reduce the temperature dynamics into

This work was supported by National Science Foundation under Grants No. 1908560 and 2050315. The opinions, findings, and conclusions or recommendations expressed are those of the author(s) and do not necessarily reflect the views of the National Science Foundation. (Corresponding author: S. Sattarzadeh). The authors thank the University of Colorado Denver for providing the battery testing facility.

S. Sattarzadeh, T. Roy, and S. Dey are with the Department of Mechanical Engineering, The Pennsylvania State University, PA 16802, USA. (e-mail: sfs6216@psu.edu, tbr5281@psu.edu, skd5685@psu.edu).

one or two states [5], [6]. However, such models are not capable of capturing the non-uniform temperature distribution which can significantly vary along length and breadth [7]–[9]. The other types of distributed thermal models are 2D models which capture the temperature distribution along length and breadth [8]–[13]; and 3D thermal models that consider the temperature distribution along length, breadth, and thickness [14]–[16]. In this work, we choose a 2D thermal model for our study which provides enough temperature distribution information while being computationally simpler than 3D models.

Temperature observers/estimators for single cylindrical cells and cylindrical cell-based packs have been widely explored [2], [17]–[27]. Although some of these works take temperature distribution into account, they may not be readily applicable to pouch cell estimation due to the following challenges: (i) Typically, distributed temperature estimation algorithms for cylindrical cells consider 1D models whereas pouch cell estimation should consider at least 2D models for reasonable accuracy; (ii) Sensor placement in cylindrical cells is trivial as sensor placed anywhere on the surface would generally enable full state observability. However, pouch cell sensor location is non-trivial due to the 2D nature of distribution. Hence, additional investigation is required for pouch cell temperature distribution estimation.

A few works exist that explore temperature estimation or sensor placement in pouch cells or geometrically similar packs. In [28], a lumped thermal model based linear Kalman filter is utilized for temperature estimation. However, it does not estimate the temperature distribution. In [29], a lumped thermal model based polytopic observer is used to estimate the temperature of sensor, cell and case in a battery pack, however, assuming uniform temperature for cell. The approach in [30] estimated the temperature of battery pack with Kalman filter. However, this approach assumes uniform heat generation which may not be satisfied in real applications. Furthermore, optimal sensor placement is not considered in this work. In [31], heat generation rate in pouch cells is investigated. The work in [32] employs the equivalent electrical representation of the thermal model for virtual temperature sensor placement and subsequently used linear Kalman filter for estimation. However, such modeling approach resulted in the requirement of twelve sensors which may not be cost effective in practical applications. In [33], the authors considered the observability of encased battery pack and investigates the optimal sensor

1

placement utilizing trace and eigen projection methods. In [34], a sensor placement strategy for 2D thermal model is used based on eigen-modes for the battery pack. However, temperature estimation problem is not considered in [33] and [34]. In summary, one or more the following research gaps exist with respect to pouch cell temperature distribution estimation. First, the minimal sensor set for single pouch cell is not explored from real-time application viewpoint. Second, sensor placement strategies are explored mostly for battery packs whereas similar investigation is lacking for single pouch cells. Finally, the estimation algorithms did not consider the case when there is just one sensor available, rendering the system unobservable.

In order to extend the aforementioned research, the main contribution of this work is an unified framework that combines the following aspects: (i) optimal sensor placement framework for pouch cells considering a 2D thermal model with non-uniform heat generation, and (ii) observer design for distributed temperature estimation in pouch cells under two scenarios: *Scenario 1* where multiple temperature sensors are available, *Scenario 2* where only one temperature sensor is available, and the proposed framework is aided by theoretical analysis along with simulation and experimental studies demonstrating its efficacy.

Scenario 2, i.e. single sensor case, is relevant to common applications with hardware cost limitations such as passenger automotive. Scenario 1 with multiple sensors, although less common, is applicable to highly safety critical applications and and high risk environments where hardware cost is not an issue. Two motivating examples of such safety critical applications are: (i) battery-powered oil-tank inspection drones [35] where safety objective is likely to dominate the sensor cost given the risk of tank explosion in case of battery failures; (ii) battery-powered mine robots [36] where thermal safety is extremely critical given the risk of explosion within the mines. The rest of paper is organized as follows: section II represents the battery thermal model, section III and section IV describes the sensor placement strategy and observer design and estimation algorithm for two different case studies, respectively. Section V represents the experimental model identification, section VI presents the simulation studies and section VII represents the experimental results and discussions. The paper is concluded in section VIII.

II. POUCH CELL THERMAL MODEL

In this work, we consider a rectangular pouch cell of dimension $a \times b \times d$. We assume a reference system of length a along x-axis, b along y-axis and the width d along the z-axis. Since the length of d is negligible compared to a and b, the temperature distribution along the z-axis is assumed to be instantaneous and uniform [9]. Hence, we are only interested in the distributed parameter model of heat transfer in two-dimension for this cell. Accordingly, a 2D thermal model for a rectangular pouch cell is adopted based on volumetric energy balance [9]. The temperature distribution T(x, y, t) in the two

dimensions x and y of the cell is given by the following twodimensional parabolic Partial Differential Equation (PDE) [9]:

$$\frac{\partial T}{\partial t} = \frac{k}{\rho C_p} \left[\frac{\partial^2 T}{\partial x^2} + \frac{\partial^2 T}{\partial y^2} \right] + \frac{Q_{heat}}{\rho C_p} - \frac{Q_{trans}}{\rho C_p v}, \tag{1}$$

where k is the average thermal conductivity of the cell assembly in the direction of the electrode surface in $Wm^{-1}K^{-1}$, ρ represents the average density of the cell components in kg/m^3 with C_p as its average specific heat capacity in $Jkg^{-1}K^{-1}$ and t is the time evolved in s. The term $Q_{heat}(x,y,t)$ is the aggregated rate of volumetric heat generation in cell due to the applied current and term Q_{trans} is the heat dissipates from battery, which are defined as follows:

$$Q_{heat}(x, y, t) = \left(E_0 - V_C - T\frac{dE_0}{dT}\right) \frac{\alpha(x, y)I}{v}, \quad (2)$$

$$Q_{trans} = h_{eff} A_s (T - T_{\infty}), \ \dot{SOC} = -\frac{I}{Q_b}, \tag{3}$$

where $E_0 = E_0(SOC)$ in Volt (V) represents the open circuit voltage as a function of $SOC \in [0, 1]$ (State-of-Charge computed via Coulomb-counting); and V_C is the terminal voltage of the battery pouch cell in Volt (V). Moreover, I in Ampere (A) represents the battery cell current (I < 0 being charge), v is cell volume in m^3 and Q_b is the capacity of battery in Ampere-seconds (A-s). The term $\frac{dE_0}{dT}$ is entropic heat generation coefficient (which is generally SOC-dependent), and A_s is cell area $(a \times b)$ in m^2 . The h_{eff} is the effective heat transfer coefficient in $(Wm^{-2}K^{-1})$, and the function $\alpha(x,y)$ captures the non-uniform heat generation along x and y axes, in the pouch cell. The PDE model (1) captures the temperature distribution given some heat input. However, the heat distribution itself is non-uniform in pouch cells due to non-uniform current distribution, as studied in existing literature [1], [37]. This non-uniform current is due to the positive and negative electrodes configurations, their active materials and electrochemical reactions inside the battery [37], [38]. To capture such non-uniform spatial heat distribution, we have used the function $\alpha(x,y)$ which is multiplied with the current in (2).

The four convective boundary conditions for this thermal model are given as follows:

$$\left. \frac{\partial T}{\partial x} \right|_{x=x_i} = \gamma_i \Big(T(x_i, y, t) - T_{\infty} \Big), \ i \in \{1, 2\}, \tag{4}$$

$$\left. \frac{\partial T}{\partial y} \right|_{y=y_j} = \gamma_j \Big(T(x, y_j, t) - T_\infty \Big), \ j \in \{3, 4\}, \tag{5}$$

where T_{∞} represents the ambient temperature, $x_1=0, x_2=a, y_3=0, y_4=b, \ \gamma_1>0, \gamma_2<0, \gamma_3>0, \gamma_4<0$ and defined as follows:

$$\gamma_1 = \gamma_3 = -\gamma_2 = \left[\frac{\delta_{case}}{k_{case}} + \frac{1}{h_1}\right]^{-1} \frac{1}{k},$$

$$\gamma_4 = -\left[\frac{\delta_{case}}{k_{case}} + \frac{1}{h_2}\right]^{-1} \frac{1}{k}$$
(6)

where δ_{case} is thickness of the battery case in m, k_{case} in $(Wm^{-1}K^{-1})$ is the thermal conductivity of the battery

casing, and h_1 and h_2 are convective heat transfer coefficients in $(Wm^{-2}K^{-1})$ along the boundaries.

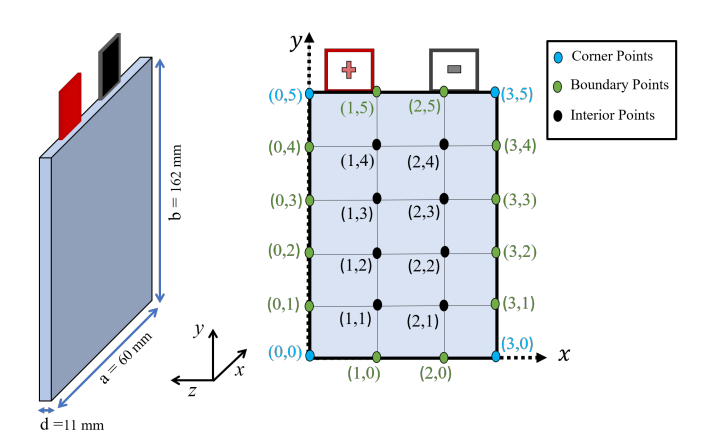


Fig. 1: Schematic of the pouch cell.

Next, we approximate (1)-(5) by a set of ODEs using the method of lines where the spatial derivatives are approximated using finite difference resulting a set of ODEs in time t. We first discretize the 2D spatial domain on this pouch cell into $(\mathcal{M}+1)\times(\mathcal{N}+1)$ grid points. The temperature at any node (m,n) in this grid is then denoted by $T_{m,n}, \forall 0 \leqslant m \leqslant \mathcal{M}, 0 \leqslant n \leqslant \mathcal{N}.$ Accordingly, the size of each cell in this grid is $\Delta_x \times \Delta_y$, where $\Delta_x = a/\mathcal{M}$ and $\Delta_y = b/\mathcal{N}.$ An example arrangement of the nodes is shown in Fig. 1 for $\mathcal{M}=3, \mathcal{N}=5.$ In method of lines, we expressed the first and second order spatial derivatives as $\frac{\partial T_{m,n}}{\partial x} \approx \frac{T_{m+1,n}-T_{m-1,n}}{2\Delta_x}$ and $\frac{\partial^2 T_{m,n}}{\partial x^2} \approx \frac{T_{m+1,n}-2T_{m,n}+T_{m-1,n}}{\Delta_x^2}$ in x dimension and followed the same approximation for y-dimension. Applying these approximations to (1), for $0 < m < \mathcal{M}, 0 < n < \mathcal{N},$ we get

$$\frac{dT_{m,n}}{dt} = \frac{k}{\rho C_p} \left[\frac{T_{m+1,n}}{\Delta_x^2} + \frac{T_{m-1,n}}{\Delta_x^2} + \frac{T_{m,n+1}}{\Delta_y^2} + \frac{T_{m,n-1}}{\Delta_y^2} - 2\left(\frac{1}{\Delta_x^2} + \frac{1}{\Delta_y^2}\right) T_{m,n} \right] + \frac{Q_{m,n}}{\rho C_p} - \frac{q_{m,n}}{\rho C_p v}, \quad (7)$$

where $Q_{m,n} = Q_{heat}(m\Delta_x, n\Delta_y)$ and $q_{m,n} = Q_{trans}(m\Delta_x, n\Delta_y)$ denotes the heat generation and dissipated heat at grid point (m, n), respectively. We follow a similar approach for the boundary grid points and corner points. In summary, we end up with $(\mathcal{M}+1)\times(\mathcal{N}+1)$ ODEs which are to be expressed as a linear state-space model. Accordingly, we define $(\mathcal{M}+1)\times(\mathcal{N}+1)$ states $[T_{0,0},T_{1,0},T_{2,0},\ldots,T_{\mathcal{M},\mathcal{N}}]$. Denoting $(\mathcal{M}+1)$ as M and $(\mathcal{N}+1)$ as N, this produces a state-space model given by:

$$\dot{x} = Ax + Bu, \ y = Cx + Du, \tag{8}$$

where $x = [x_1, x_2, ..., x_{MN}]^T \in \mathbb{R}^{MN}$, with $x_i = T_{m,n}$ and $u = [u_1, u_2]^T \in \mathbb{R}^{MN+1}$ with $u_1 = Q_{m,n}$ and $u_2 = T_{\infty}$; $y = [y_1, y_2, ..., y_p]^T \in \mathbb{R}^p$ is the measured output vector assuming

p temperature sensors are used. The state-space matrices are given for M=3 and N=4 by:

$$A = \frac{k}{\rho C_p} \begin{bmatrix} a_1 & \frac{2}{\Delta_x^2} & 0 & \frac{2}{\Delta_y^2} & 0 & 0 & 0 & 0 & 0 & 0 & 0 & 0 \\ \frac{1}{\Delta_x^2} & a_2 & \frac{1}{\Delta_x^2} & \frac{2}{\Delta_x^2} & 0 & 0 & 0 & 0 & 0 & 0 & 0 & 0 \\ 0 & \frac{2}{\Delta_x^2} & a_3 & 0 & 0 & \frac{2}{\Delta_y^2} & 0 & 0 & 0 & 0 & 0 & 0 & 0 \\ \frac{1}{\Delta_y^2} & 0 & 0 & a_4 & \frac{2}{\Delta_x^2} & 0 & \frac{1}{\Delta_y^2} & 0 & 0 & 0 & 0 & 0 & 0 \\ 0 & \frac{1}{\Delta_y^2} & 0 & \frac{1}{\Delta_x^2} & a_5 & \frac{1}{\Delta_y^2} & 0 & 0 & 0 & 0 & 0 \\ 0 & 0 & \frac{1}{\Delta_y^2} & 0 & \frac{1}{\Delta_x^2} & a_5 & \frac{1}{\Delta_y^2} & 0 & 0 & 0 & 0 & 0 \\ 0 & 0 & \frac{1}{\Delta_y^2} & 0 & \frac{2}{\Delta_x^2} & a_6 & 0 & 0 & \frac{1}{\Delta_y^2} & 0 & 0 & 0 & 0 \\ 0 & 0 & 0 & \frac{1}{\Delta_y^2} & 0 & 0 & a_7 & \frac{2}{\Delta_x^2} & 0 & \frac{1}{\Delta_y^2} & 0 & 0 & 0 \\ 0 & 0 & 0 & 0 & \frac{1}{\Delta_y^2} & 0 & 0 & a_7 & \frac{2}{\Delta_x^2} & 0 & \frac{1}{\Delta_y^2} & 0 & 0 & 0 \\ 0 & 0 & 0 & 0 & \frac{1}{\Delta_y^2} & 0 & \frac{1}{\Delta_x^2} & a_8 & \frac{1}{\Delta_x^2} & 0 & \frac{1}{\Delta_y^2} & 0 & 0 \\ 0 & 0 & 0 & 0 & 0 & 0 & \frac{1}{\Delta_y^2} & 0 & \frac{2}{\Delta_x^2} & a_9 & 0 & 0 & \frac{1}{\Delta_y^2} \\ 0 & 0 & 0 & 0 & 0 & 0 & 0 & 0 & \frac{2}{\Delta_y^2} & 0 & \frac{1}{\Delta_x^2} & a_{11} & \frac{1}{\Delta_x^2} \\ 0 & 0 & 0 & 0 & 0 & 0 & 0 & 0 & \frac{2}{\Delta_y^2} & 0 & \frac{1}{\Delta_x^2} & a_{11} & \frac{1}{\Delta_x^2} \\ 0 & 0 & 0 & 0 & 0 & 0 & 0 & 0 & 0 & \frac{2}{\Delta_y^2} & 0 & \frac{2}{\Delta_x^2} & a_{12} \end{bmatrix}$$

$$\begin{aligned} a_1 &= -2 \left[\frac{1}{\Delta_x^2} + \frac{1}{\Delta_y^2} + \frac{\gamma_3}{\Delta_y} + \frac{\gamma_1}{\Delta_x} \right] + H, & a_2 &= -2 \left[\frac{1}{\Delta_x^2} + \frac{1}{\Delta_y^2} + \frac{\gamma_3}{\Delta_y} \right] + H, \\ a_3 &= -2 \left[\frac{1}{\Delta_x^2} + \frac{\gamma_3}{\Delta_y^2} + \frac{\gamma_3}{\Delta_y} - \frac{\gamma_2}{\Delta_x} \right] + H, & a_4 &= a_7 &= -2 \left[\frac{1}{\Delta_x^2} + \frac{1}{\Delta_y^2} + \frac{\gamma_1}{\Delta_x} \right] + H, \\ a_5 &= a_8 &= -2 \left[\frac{1}{\Delta_x^2} + \frac{1}{\Delta_y^2} \right] + H, & a_6 &= a_9 &= -2 \left[\frac{1}{\Delta_x^2} + \frac{1}{\Delta_y^2} - \frac{\gamma_2}{\Delta_x} \right] + H, \\ a_{10} &= -2 \left[\frac{1}{\Delta_x^2} + \frac{1}{\Delta_y^2} - \frac{\gamma_4}{\Delta_y} + \frac{\gamma_1}{\Delta_x} \right] + H, & a_{11} &= -2 \left[\frac{1}{\Delta_x^2} + \frac{1}{\Delta_y^2} - \frac{\gamma_4}{\Delta_y} \right], \\ a_{12} &= -2 \left[\frac{1}{\Delta_x^2} + \frac{1}{\Delta_y^2} - \frac{\gamma_4}{\Delta_y} - \frac{\gamma_2}{\Delta_x} \right] + H, \end{aligned}$$

where $H=-A_sh_{eff}$ and the last column in B matrix corresponds to the second input which is T_{∞} and is obtained based on the boundary conditions in (4)-(5). The D matrix is zero and the C matrix can be obtained based on sensor placement strategy.

Note that we formulated the state-space model to achieve a Linear Time-Invariant (LTI) form. Such linear form will essentially enable the utilization of standard LTI techniques for analysis and design. We have treated the heat generation $(Q_{m,n})$ as a known input to the system to ensure such LTI form. This is enabled by the assumption that the entropic heat is negligible. In practical implementation, such heat generation can be computed online via (2) utilizing the following information: (i) measured terminal voltage and current, (ii) estimated SOC via Coulomb counting or closed-loop SOC estimator, and (iii) experimentally identified $\alpha(x,y)$. This assumption enabled us to bypass the input nonlinearity associated with $Q_{m,n}$ term.

Several factors should be considered while determining the number of grid points in discretization. A major factor is the condition number of A matrix. The condition number

is defined by the ratio of maximum singular value to the minimum singular value of the matrix. As discussed in [39], larger condition number may lead to the following issues: (i) small perturbations in system parameters may move the system towards numerical instability, and (ii) the observability of a system with few sensors becomes challenging. Furthermore, large number of states may also add to computational complexity of the model and the algorithm. Having excessively finer discretization may lead to the following issues: (i) it may not provide additional useful information as temperature variation along some adjacent points would be negligible in such scenario, and (ii) owing to the physical space taken by the sensor, it may not be feasible to place sensor on a node as that particular node may not be practically distinguishable from its adjacent nodes. Hence, all these factors limits the maximum number of grid points. On the other hand, choosing too small number of grid points leads to the sparse model which may not represent the PDE properly and some information of the system may be lost. In summary, choice of number of grid points is (i) motivated by the trade-off between accuracy, numerical stability, and computational complexity, and (ii) dictated by sensor installation limits, dimension of battery, and the temperature variation along the cell [32].

III. OPTIMAL SENSOR LOCATIONS

In this section, we discuss optimal sensor placement for two scenarios: (i) when it is feasible to embed multiple sensors, and (ii) when only one sensor is feasible. Multiple sensors can be feasible for applications that are highly safety critical whereas single sensor case are for more common applications where cost effectiveness play a significant role. To begin with, we define the observability Gramian as state observability metric [40]:

$$W_o = \int_0^\infty e^{A^T t} C^T C e^{A^T t} dt, \tag{12}$$

where W_o is obtained by solving the continuous-time Lyapunov equation:

$$A^T W_o + W_o A = -C^T C. (13)$$

If the A matrix has all the eigen values with negative real part, the Lyapunov solution is a positive definite matrix and system is observable. In other words, the system is observable if the W_o matrix is non-singular. Furthermore, the trace of W_o , given by $\operatorname{tr}(W_o) = \sum_{i=1}^{MN} \sigma_i(W_o)$ where σ_i indicates the i-th eigen value, provides a measure for degree of observability. That is, larger trace of W_o implies the greater observability [40], [41]. Next, we discuss the sensor placement for two aforementioned scenarios.

A. Multiple sensor case

In this case, our goal is to find minimum number of sensors and their locations that would result in full state observability. We achieve this in two steps. First, following the approach presented in [42], we find the minimum number of sensors by evaluating the singular values of the Gramian matrix W_o in (12). Essentially, we find the minimum number of singular

values that contain majority amount of information which in turn give us the minimum number of sensors required for system observability. We first order the singular values in a descending manner. Then we compute the following metric d_i for i-th singular value, starting from the second highest singular value and moving in a descending order.

$$d_i = 100 \times \frac{\sigma_i - \sigma_{i+1}}{\sigma_i}. (14)$$

Here d_i indicates the percentage change in adjacent singular values. Subsequently, we choose minimum number of sensors $K_{opt} = n$ based on the condition $d_n < \beta$ where β is a predetermined threshold. In this work, we have used $\beta = 50\%$.

In order to verify the outcome of the SVD approach, we have utilized an alternate method to compute the minimum number of sensors. We solve the following optimization problem:

$$\min_{c_i \in \{0,1\}} \sum_{i=1}^{MN} c_i, \text{ subject to: } \operatorname{rank}(W_o) = MN, \tag{15}$$

where $C = [c_i] \in \mathbb{R}^{MN \times MN}$ and, C is constrained to have only one entry of 1 in each row. In our case studies, the SVD approach and this alternate method resulted in same outcome.

Next, we find the locations of the sensors which provide full observability. To achieve this, we formulate the optimal sensor placement problem as follows [43]:

$$\max_{c_i \in \{0,1\}} \operatorname{tr}(W_o),$$
subject to:
$$\sum_{i=1}^{MN} c_i = K_{opt}, \quad \operatorname{rank}(W_o) = MN \qquad (16)$$

where K_{opt} is the number of sensors found in previous step, $c_i=1$ indicates presence of sensor whereas $c_i=0$ indicates no sensor, and W_o is the solution of (13) with $C=[c_i]\in\mathbb{R}^{K_{opt}\times MN}$. Furthermore, C is constrained to have only one entry of 1 in each row. Essentially, the objective is to maximize the trace of W_o by varying the locations of the sensors.

B. Single sensor case

In this case, we consider the scenario where it is not feasible to install multiple sensors due to cost or other constraints. Under this scenario, we will not be able to achieve full state observability if we have a large number of states. Accordingly, our goal is here is to find that particular sensor location which provides maximum possible degree of observability. In order to achieve this, we formulate the following optimization problem:

$$\max_{c_i \in \{0,1\}} \text{ tr}(W_o), \text{ subject to: } \sum_{i=1}^{MN} c_i = 1,$$
 (17)

where W_o is the solution of (13) with $C = [c_i] \in \mathbb{R}^{1 \times MN}$, and $c_i = 1$ indicates presence of sensor whereas $c_i = 0$ indicates no sensor. Furthermore, C is constrained to have only one entry of 1.

IV. OBSERVERS FOR DISTRIBUTED TEMPERATURE ESTIMATION

In this section, we design robust estimation algorithms to estimate the 2D distributed temperature of pouch cells.

A. Observer design with multiple sensors

In this case, the system is fully observable and we construct a sliding mode based [44], [45] robust observer given by:

$$\dot{\hat{x}} = A\hat{x} + Bu + L_1(y - \hat{y}) + L_2 \frac{(y - \hat{y})}{\|y - \hat{y}\|}, \ \hat{y} = C\hat{x}, \quad (18)$$

where ||.|| represents \mathcal{L}_2 vector norm, $L_1 \in \mathbb{R}^{MN \times p}$ and $L_2 \in \mathbb{R}^{MN \times p}$ are constant observer gains. We can write the error dynamic by subtracting (18) from (8):

$$\dot{e} = (A - L_1 C)e - L_2 \frac{Ce}{\|Ce\|},$$
 (19)

where $e = x - \hat{x}$. Next, the following proposition explains the convergence of error dynamics.

Proposition 1. Consider the error dynamics (19) If L_1 is chosen such that $(A - L_1C)^TP + P(A - L_1C) < 0$ where P is a symmetric positive definite matrix, and $L_2 = \gamma P^{-1}C^T$ with $\gamma > 0$, then the estimation error will converge to zero as $t \to \infty$

Proof. The proposition can be proved following the approaches outlined in [45], [46]. A choice of Lyapunov function candidate $V = e^T P e$ and $L_2 = \gamma P^{-1} C^T$ leads to

$$\dot{V} = e^T [(A - L_1 C)^T P + P(A - L_1 C)]e - 2\gamma \|Ce\|.$$

Choosing L_1 such that $(A - L_1C)^T P + P(A - L_1C) < 0$, and choosing $\gamma > 0$ such that $-2\gamma \|Ce\| < 0$, we have $\dot{V} < 0$ which leads to convergence of e to zero as $t \to \infty$.

B. Observer design with single sensor

As we have only one sensor, the system states are not fully observable in this case. To deal with such observability issue, we first decompose the original unobservable system (8) into observable and unobservable subsystems utilizing the Kalman decomposition [47] with the state transformation $\bar{x} = Tx$ where T is the transformation matrix. The transformed system is given by:

$$\dot{\bar{x}} = \overline{A}\bar{x} + \overline{B}u \tag{20}$$

$$y = \overline{C}\bar{x},\tag{21}$$

where

$$\bar{x} = \begin{bmatrix} \overline{x}_1 \\ \overline{x}_2 \end{bmatrix}, \overline{A} = \begin{bmatrix} A_{un} & A_{12} \\ 0 & A_{ob} \end{bmatrix}, \overline{B} = \begin{bmatrix} B_{un} \\ B_{ob} \end{bmatrix}$$

$$\overline{C} = \begin{bmatrix} 0 & C_{ob} \end{bmatrix}$$
(22)

Here, $\overline{x}_1 \in \mathbb{R}^{(MN-r)}$ is unobservable state vector and $\overline{x}_2 \in \mathbb{R}^r$ observable state vector. If the pair (A_{ob}, C_{ob}) is observable and A_{un} is asymptotically stable then it is possible to design an observer for the entire system. If these two conditions hold, the system is detectable [48]. Subsequently, we utilize a cascade scheme where a first sub-estimator estimates the observable

states and these estimated observable states are fed into a second sub-estimator. The second sub-estimator estimates the full system states using the information from the first sub-estimator as output feedback.

We choose the structure of the first sub-estimator as:

$$\begin{bmatrix}
\hat{\bar{x}}_1 \\
\hat{\bar{x}}_2
\end{bmatrix} = \begin{bmatrix}
A_{un} & A_{12} \\
\mathbf{0} & A_{ob}
\end{bmatrix} \begin{bmatrix}
\hat{\bar{x}}_1 \\
\hat{\bar{x}}_2
\end{bmatrix} + \begin{bmatrix}
B_{un} \\
B_{ob}
\end{bmatrix} u \\
+ \begin{bmatrix}
\mathbf{0} \\
L_3
\end{bmatrix} (y - \hat{y}) + \begin{bmatrix}
\mathbf{0} \\
L_4
\end{bmatrix} \frac{y - \hat{y}}{\|y - \hat{y}\|} \\
\hat{y} = \begin{bmatrix}
\mathbf{0} & C_{ob}
\end{bmatrix} \begin{bmatrix}
\hat{\bar{x}}_1 \\
\hat{\bar{x}}_2
\end{bmatrix}, C_{ob} = \begin{bmatrix}
0 & 0 & 0 & \dots & 1
\end{bmatrix}, (23)$$

where L_3 and L_4 are estimator gains. The second subestimator structure is given by

$$\frac{\dot{\bar{x}}}{\hat{x}_n} = \overline{A}\hat{\bar{x}}_n + \overline{B}u + L_5(y_m - \hat{\bar{y}}) + L_6 \frac{y_m - \hat{\bar{y}}}{\|y_m - \hat{\bar{y}}\|}
\hat{\bar{y}} = \begin{bmatrix} \mathbf{0} & C_{new} \end{bmatrix} \hat{\bar{x}}_n, \ C_{new} = \begin{bmatrix} 1 & 1 & 1 & \dots & 1 \end{bmatrix}, \quad (24)$$

where $y_m = \hat{x}_2$ from the first sub-estimator, \hat{x}_n is the estimated full state vector, and L_5 and L_6 are estimator gains. Finally, the state estimates in original domain are computed as $\hat{x} = T^{-1}\hat{x}_n$. The convergence of the first and second sub-estimators can be proved following a similar approach as in Proposition 1.

V. EXPERIMENTAL IDENTIFICATION AND OPTIMAL SENSOR PLACEMENT

In this section, we present the experimental identification of 2D thermal model and optimal sensor placement for a commercial pouch type cell. The commercial pouch type cell has rated capacity of 10 Ah, maximum charge cut-off voltage 4.2 ± 0.05 V, and discharge cut-off voltage 2.75 V. An Arbin battery tester (model BT-2000) is used to perform the battery experiments. The experimental setup is illustrated in Fig. 2 where five K-type thermocouples are installed on the pouch cell to collect distributed temperature data. As shown in Fig. 1, we chose M=4 and N=6 to capture the temperature distribution on pouch cell. Accordingly, we have 24 nodes or states in the state-space model (8). It should be noted that by choosing M = 4 and N = 6, the grid step size becomes $\Delta_x = 20 \ mm$ and $\Delta_y = 32.4 \ mm$, which provides a reasonable number of grid points with respect to the battery size, sensor installation limits and temperature variation along the cell. Comparing Fig. 1 and Fig. 2, we denote S_1 = $T_{1,1}, S_2 = T_{2,1}, S_3 = T_{1,4}, S_4 = T_{2,4}, S_5 = T_{1,5}$, respectively.

We utilized the experimental measurements including terminal voltage, current and temperatures to identify the unknown parameters of the model discussed in Section II. The OCV-SOC map was identified based on a constant current rate of C/30 by cycling the battery from SOC=1 to SOC=0 and shown in Fig. 5a. Subsequently, we solved the following optimization problem: $\min_{\vartheta \in [\underline{\vartheta}, \overline{\vartheta}]} \text{RMS}(T_{exp} - T_{model}(\vartheta))$ with respect to dynamic constraints (8). Here, $\vartheta = \{Q_b, h_1, h_2, k_{case}, C_p, k\}$ is the unknown parameters vector, the RMS(.) is the root mean square operator, and T_{exp}

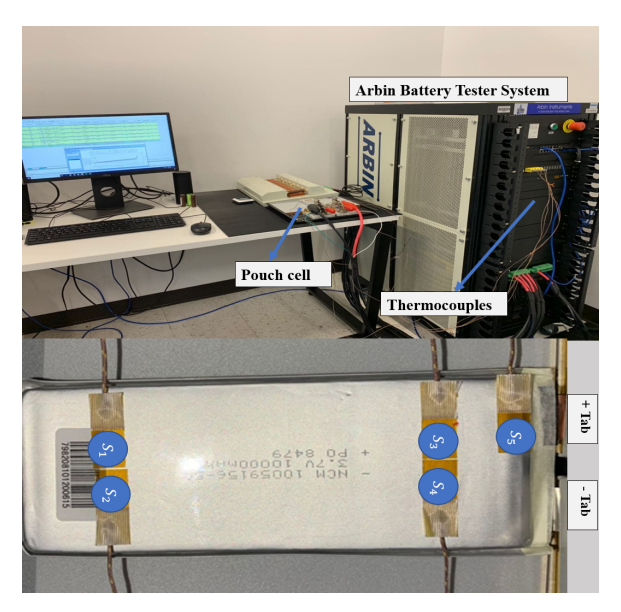


Fig. 2: The experimental setup with the five surface thermocouples. The blue circles on battery demonstrate the sensor locations.

and T_{model} are the experimental temperature and the model temperature, respectively. Furthermore, ϑ and $\overline{\vartheta}$ are parameter bounds. Such optimization is performed with experimental data under 5C and modified US06 type current profiles (shown in Fig. 3) utilizing Genetic optimization Algorithm (GA). The identification results are given in Table I. Subsequently, we have identified the function $\alpha(x,y)$ utilizing a discretized form to further minimize the error between model output and experimental data. The discretized function is parameterized by $\alpha_{mn} = \alpha(m\Delta_x, n\Delta_y)$ which are subsequently treated as design variables to minimize RMS $(T_{exp} - T_{model}(\alpha_{mn}))$. The identified function is shown in Fig. 5b. Other parameters are taken directly from the cell datasheet and literature [9]: $m = 0.2 \text{ kg}, \ \delta_{case} = 162 \times 10^{-7} \text{ m}, \ \rho = 1.87 \times 10^{-3}$ kgm^{-3} and natural convection $h_{eff}=5\ Wm^{-2}K^{-1}.$ As per our model formulation, we have considered $\frac{dE_0}{dT} \approx 0$. After identification, we evaluate the performance of identified model using a modified UDDS type current profile (shown in Fig. 3). The RMS errors for identification and validation current profiles are given in Table II. The model accuracy for S_5 is illustrated in Fig. 4 as a sample to demonstrate the model performance.

TABLE I: Identified parameters

Parameters	Values	Parameters	Values
$\overline{Q_b}$	10.1 Ah	k_{case}	$0.16 \ Wm^{-1}K^{-1}$
h_1	$48 \ Wm^{-2}K^{-1}$	h_2	$14 \ Wm^{-2}K^{-1}$
C_p	$1019.99 \ Jkg^{-1}K^{-1}$	k	$5.99 \ Wm^{-1}K^{-1}$

Next, we present the results of optimal sensor placement approaches discussed in Section III. First, we discuss the multiple sensor case. The singular values of the experimentally identified model are shown in Fig. 6. Based on the discretization discussed in previous section, we have 24 states and hence 24 singular values. As we can see from Fig. 6, by choosing

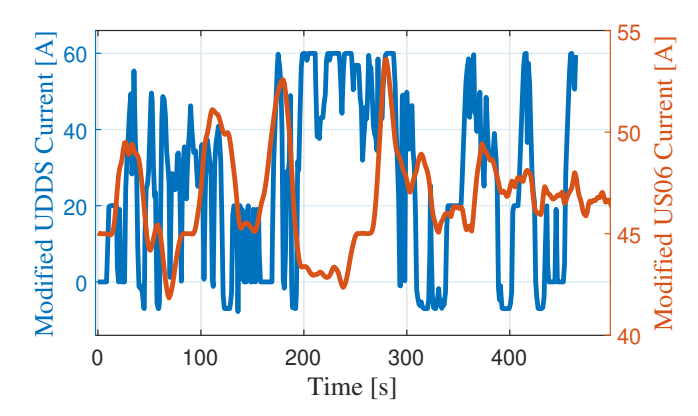


Fig. 3: Modified UDDS and US06 current profiles.

TABLE II: RMS errors of model identification and validation

RMS errors in ^o C under different current profiles				
Location	US06 current	5C current	UDDS current	
S_1	0.1866	0.4448	0.6615	
S_2	0.3354	0.3607	0.7130	
S_3	0.3426	0.4284	0.7866	
S_4	0.3396	0.3660	0.7196	
S_5	0.1975	0.3714	0.5545	

the threshold as $\beta = 50\%$, the first three singular values contain majority of the information about the system. On the other hand, by solving the optimization problem in (15) for MN = 24, we obtain three sensors as a solution of optimization algorithm. Accordingly, we need at least three sensors that can provide full state observability, that is $K_{opt} = 3$. Next step is to find the optimal locations of these three sensors. For this purpose, we use Genetic Algorithm to solve the sensor placement optimization problem (16) discussed in Section III. Subsequently, we found that having sensors on locations $S_1 = T_{1,1}$, $S_3 = T_{1,4}$, and $S_4 = T_{2,4}$ (see Fig. 2) maximizes $tr(W_o)$. Next, we consider the single sensor case. We solved the optimization problem (17) and found that $S_4 = T_{2,4}$ is the sensor location that maximizes $tr(W_o)$. With such choice of sensor, we have 13 observable states and 11 unobservable states.

VI. SIMULATION STUDIES

In this section, we present simulation studies to evaluate the performance of the proposed observers. The 2D thermal model and the observers are implemented in MATLAB/Simulink platform. We explore two scenarios under the aforementioned modified UDDS profile: (i) multiple sensor case where the output feedback is from the nodes $S_1 = T_{1,1}$, $S_3 = T_{1,4}$, and $S_4 = T_{2,4}$, and (ii) single sensor case where the output feedback is from the node $S_4 = T_{2,4}$. For both cases, the output feedback is generated from the MATLAB simulation model. The observers are initialized with incorrect temperature values to verify convergence. The temperature distribution of 2D model along length and breadth is shown in Figs. 7a, 7b, and 7c, at different time instants. As we can see, the temperature distribution is asymmetric due to the nonuniform and asymmetric current and heat distribution which is captured by function $\alpha(x,y)$. Furthermore, the areas closer

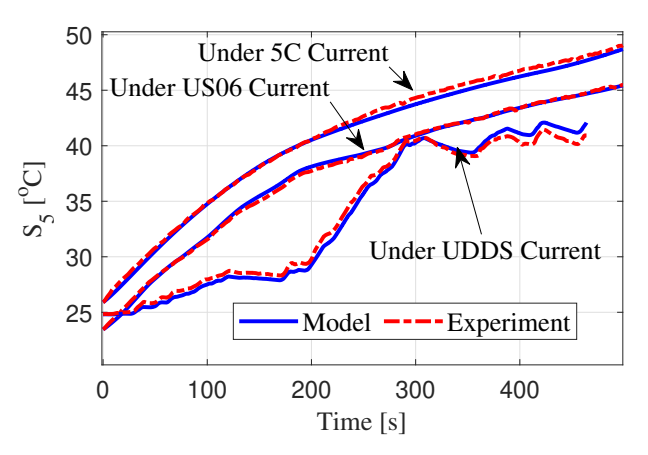


Fig. 4: Identification and validation results for node S_5 under different currents.

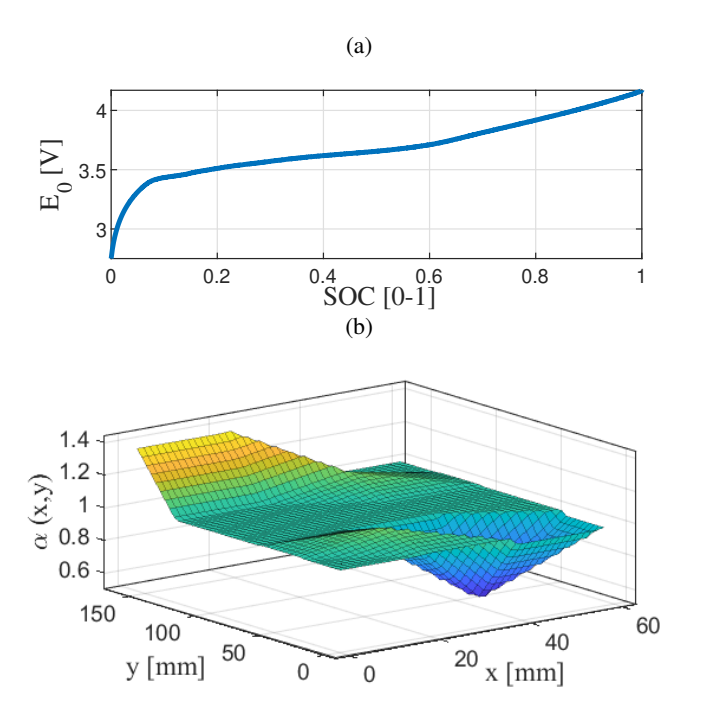


Fig. 5: The identified (a) OCV-SOC map; (b) $\alpha(x, y)$ function

to the positive tab have higher temperatures. The temperature estimation errors at 24 nodes for multiple and single sensor cases are shown in Fig. 7d. For both cases, the estimation errors converged to zero. However, it seems that multiple sensor observer is slightly more robust to sudden changes in input current. This is evident from the fact that the estimation errors in single sensor case are perturbed after 200 s whereas estimation errors in multiple sensor case show no such perturbation. We have also tested the robustness of the proposed observers under sensor noise. To illustrate the robustness, the estimation error for node S_5 is shown in Fig. 8 for multiple sensor case under different levels of measurement noise. The measurement noise injected is of white Gaussian in nature, denoted by $\mathcal{N}(0, \sigma^2)$ where σ is the standard deviation. The results show that the proposed observer was able to handle reasonable amount of measurement noise.

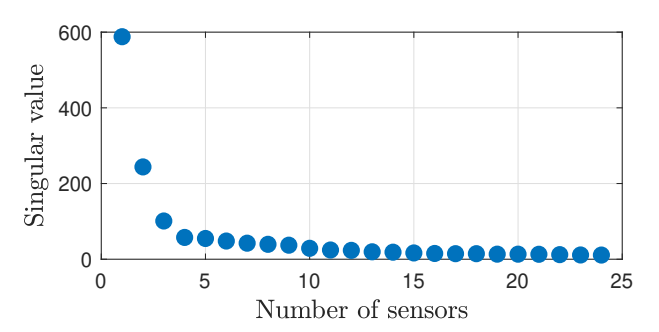


Fig. 6: The singular values of Gramian observability matrix in fully observable case with maximum number of sensors.

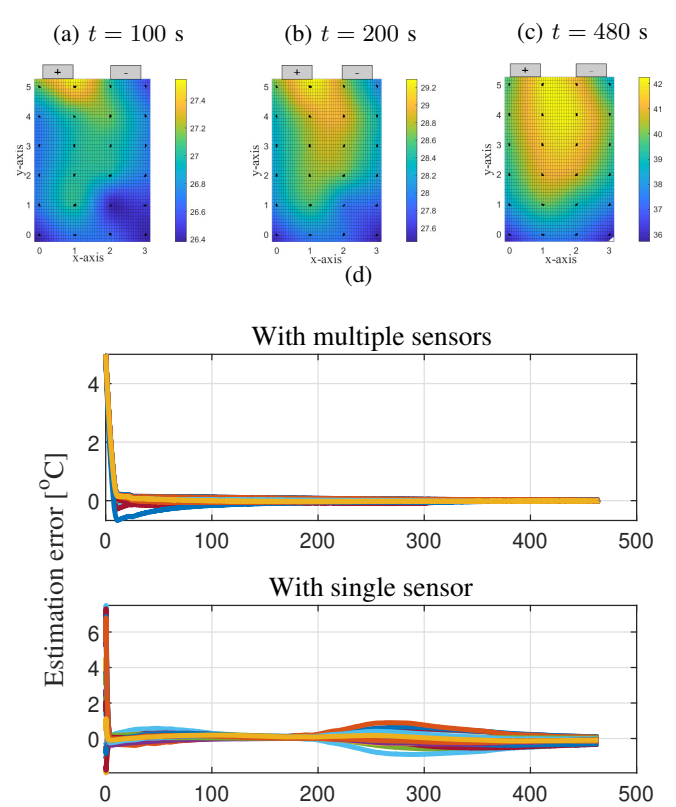


Fig. 7: Temperature distribution under modified UDDS current profile at (a) $t=100~\rm s$; (b) $t=200~\rm s$; (c) end of discharge; (d) comparison of multiple sensors and single sensor estimation errors.

Time [s]

VII. EXPERIMENTAL STUDIES

In this section, we illustrate the performance of the proposed observers based on experimental data. The experimental data is fed to the observers as output feedback. We present the following cases.

A. Multiple sensors case

In the first study, we evaluate the performance of the observer for multiple sensors case under modified US06 and UDDS current (shown in Fig. 3). Recall that we have $S_1=T_{1,1},\,S_3=T_{1,4}$, and $S_4=T_{2,4}$ as measured outputs for

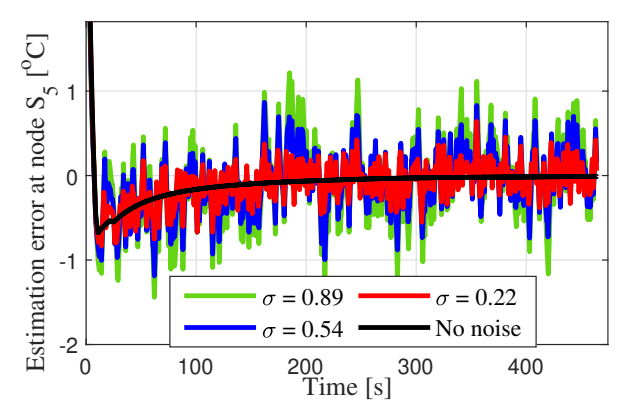


Fig. 8: Estimation result for node S_5 under different levels of measurement noise.

multiple sensors case. The estimation performance is evaluated in terms of the estimation errors at the nodes S_1 through S_5 (refer to Fig. 2). The experimental temperature and their corresponding estimates are shown in Fig. 9 and Fig. 10. In both cases, the estimates are initialized with incorrect values and eventually they converged to the true values. For US06 profile, the convergence time for these estimates is within 10 seconds and the steady-state estimation errors are within $0.45^{\circ}C$. For UDDS profile, the convergence time for these estimates is within 10 seconds and the steady-state estimation errors are within $0.87^{\circ}C$.

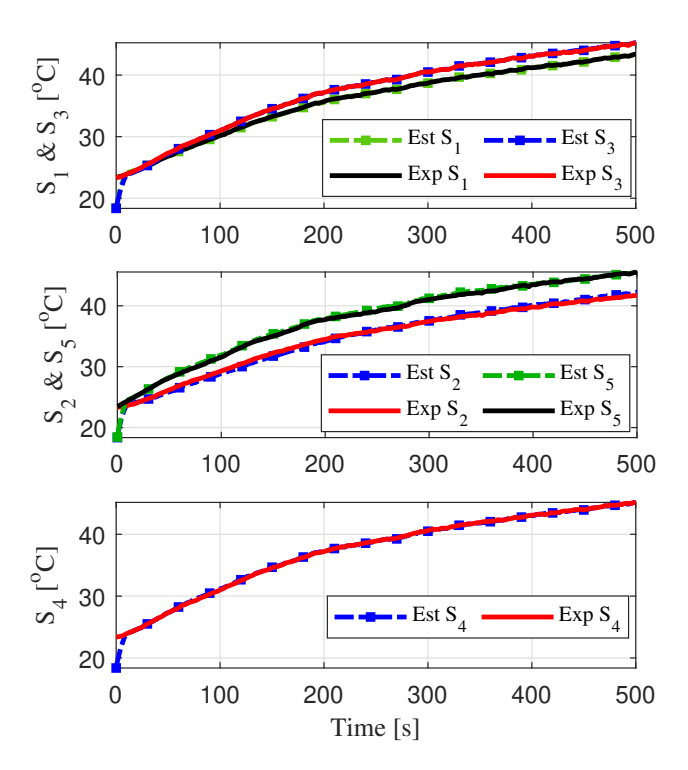


Fig. 9: Estimation result with multiple sensors under US06 current profile. *Est* indicates estimated temperature and *Exp* indicates experimental data.

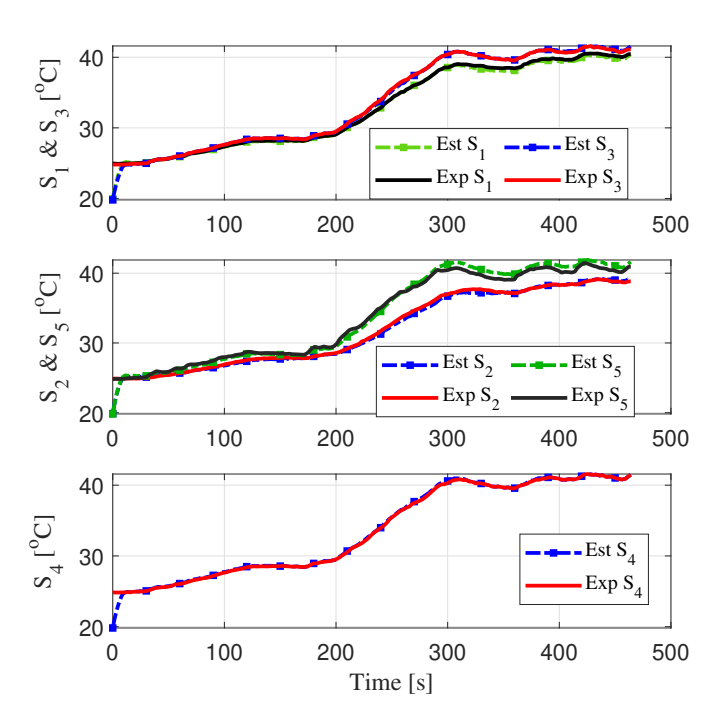


Fig. 10: Estimation result with multiple sensors under UDDS current profile. *Est* indicates estimated temperature and *Exp* indicates experimental data.

B. Single sensor case

In this case study, we evaluate the performance of the single sensor based observer under modified US06 and 5C constant current profile. Note that we have $S_4 = T_{2,4}$ as the measured output for single sensor case. Similar to the previous case, the estimation performance is evaluated in terms of the estimation errors at the nodes S_1 through S_5 . The experimental temperature and their corresponding estimates are shown in Fig. 11 and Fig. 12. In both cases, the estimates are initialized with incorrect values and eventually they converged to the true values. For US06 profile, the convergence time for these estimates is within 4 seconds and the steady-state estimation errors are within $1.18^{\circ}C$. For 5C current, the convergence time for these estimates is within 5 seconds and the steady-state estimation errors are within $1.3^{\circ}C$.

C. Robustness under uncertainties in model parameters

In this subsection, we investigate the performance of observers under parametric uncertainties. Our goal is to understand how the estimator errors are affected when certain parameters of the model are not exactly known. This is important since in practical applications such uncertainty in parameters knowledge are common due to several reasons such as manufacturing variability and packaging. To illustrate the robustness, we consider multiple sensors scenario and inject uncertainties in the parameters h_2 and C_p under modified US06 profile. The steady-state estimation errors in S_5 for different levels of uncertainties are shown in Fig. 13. We observe the following: (i) the convergence performance

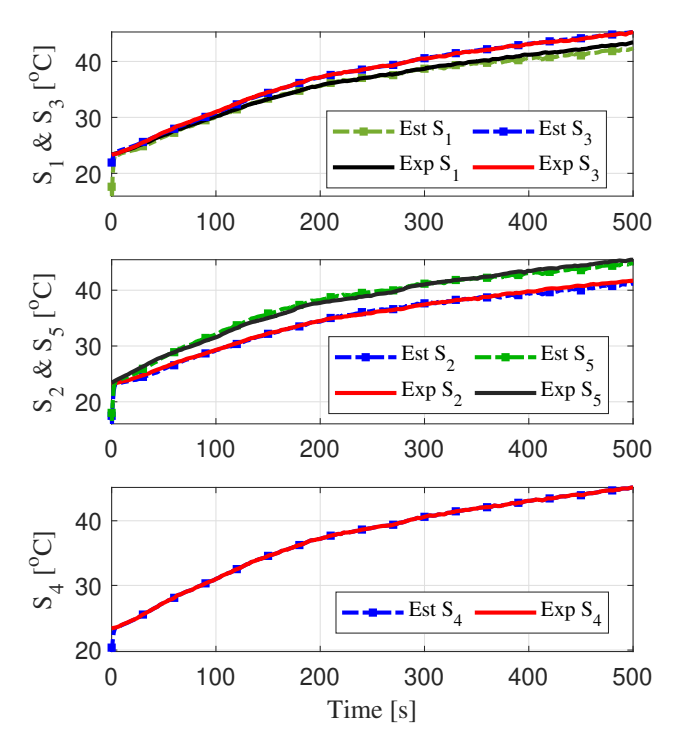


Fig. 11: Estimation result with single sensor under US06 current profile. *Est* indicates estimated temperature and *Exp* indicates experimental data.

starting from non-zero error was not affected, and (ii) the steady-state estimation errors degraded with higher level of uncertainties. Specifically, the observer performs reasonably up to 30% uncertainty in C_p and 57% uncertainty in h_2 , assuming 0.5^o C is acceptable upper bound of estimation error.

D. Comparison: multiple and single sensor cases

Here, we compare the performance of the observers in multiple sensors and single sensor cases. As a representative example, the estimation errors at node S_5 for both cases are shown in Fig. 14. The accuracy is better for the multiple sensors case, which is expected as more feedback typically leads to better estimation. However, there are some tradeoffs in terms of computational complexity and hardware cost. Single sensor observer requires only one sensor leading to less hardware cost as compared to multiple sensors case. On the other hand, the computational complexity for single sensor observer is higher due to the presence of cascade estimator scheme. Essentially, two sets of ODE observer equations need to be solved in real-time whereas in multiple sensor case we need to solve only one ODE observer equation. Furthermore, single sensor scheme is more sensitive to model uncertainties and input perturbations compared to multiple sensor case. This is due to the fact that more feedback information helps suppress disturbances better.

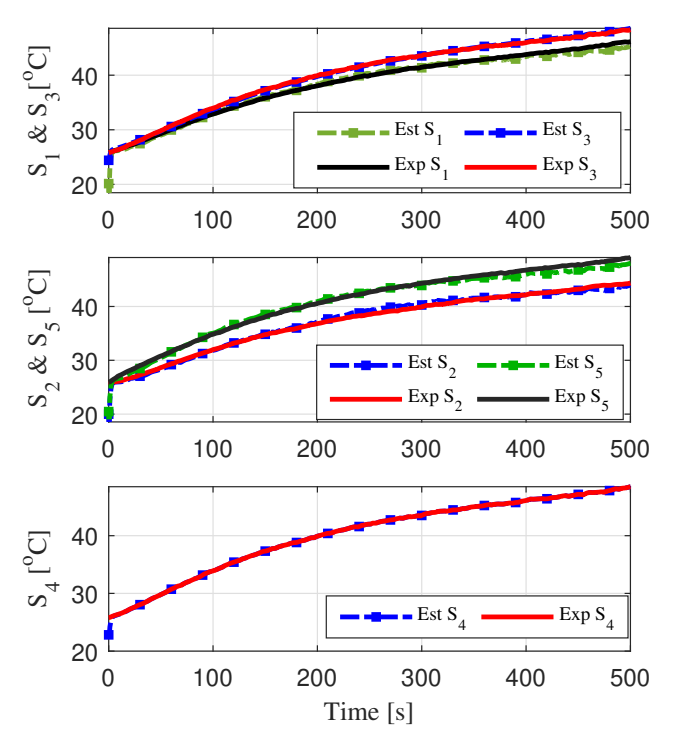


Fig. 12: Estimation result with single sensor under 5C current profile. *Est* indicates estimated temperature and *Exp* indicates experimental data.

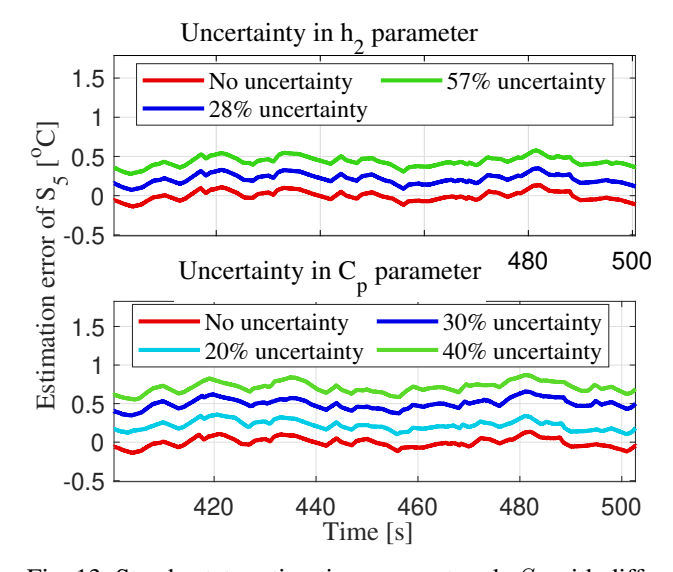


Fig. 13: Steady state estimation errors at node S_5 with different levels of uncertainties in h_2 and C_p parameters under US06 modified dynamic current.

E. Discussion

In this subsection, we discuss some general observations on the temperature distribution estimation of pouch cells. Figure 15 shows the temperature distribution for all 24 nodes under modified UDDS current profile. It is clear that the non-uniformity of temperature distribution is considerable and

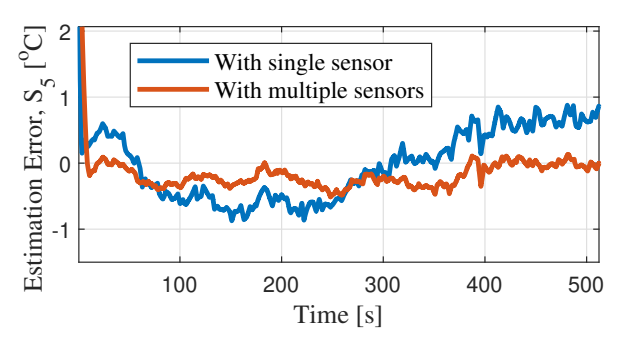


Fig. 14: Comparison of estimation errors with multiple sensors and single sensor case.

hence, confirms the importance of distributed temperature estimation. According to the modeling and estimation results, we see that the nodes closer to the tabs have higher temperatures, and we have more heat generation on the positive tab side than the negative tab side. Comparing the temperatures of nodes S_5 and S_2 , we can see the considerable difference in temperatures which indicates the importance of sensor placement for this type of cells. These studies help us to explore the temperature distribution along the pouch cell and subsequently enhances our knowledge of the critical hotspots. The estimated distributed temperature information can be useful in the following ways: (i) it can inform the thermal management strategies to achieve better thermal balancing, and (ii) it can inform the temperature dependent electrical and electrochemical parameter estimation techniques.

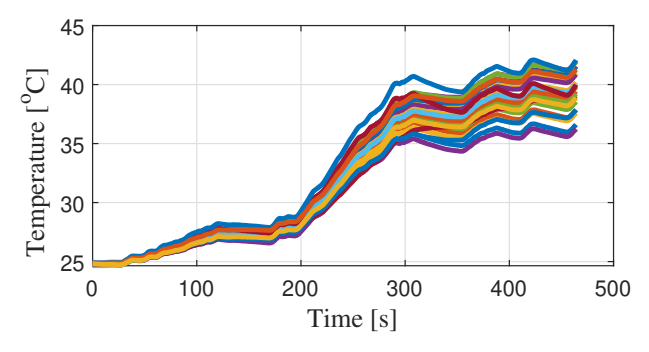


Fig. 15: Temperature distribution along the pouch cell under modified UDDS current profile.

VIII. CONCLUSION

In this paper, we discuss sensor placement strategies and estimation schemes for pouch cells. The sensor placement strategies maximize the state observability and the estimation schemes estimate distribution of temperature. We considered a 2D thermal model to capture the non-uniform temperature and heat distribution along the battery pouch cell. We explored multiple sensors and single sensor scenarios. These studies can help find the critical hot-spots on the battery and monitor them to avoid thermal runaway and faults in batteries.

REFERENCES

- [1] T. Wang, C. Li, L. Chang, B. Duan, and C. Zhang, "Thermal behavior analysis of pouch lithium ion battery using distributed electro-thermal model," in 2019 3rd Conference on Vehicle Control and Intelligence (CVCI). IEEE, 2019, pp. 1–5.
- [2] Y. Kim, S. Mohan, J. B. Siegel, A. G. Stefanopoulou, and Y. Ding, "The estimation of temperature distribution in cylindrical battery cells under unknown cooling conditions," *IEEE Transactions on Control Systems Technology*, vol. 22, no. 6, pp. 2277–2286, 2014.
- [3] J. Jaguemont, L. Boulon, and Y. Dubé, "Characterization and modeling of a hybrid-electric-vehicle lithium-ion battery pack at low temperatures," *IEEE Transactions on Vehicular Technology*, vol. 65, no. 1, pp. 1–14, 2015.
- [4] Y. Ji, Y. Zhang, and C.-Y. Wang, "Li-ion cell operation at low temperatures," *Journal of The Electrochemical Society*, vol. 160, no. 4, p. A636, 2013.
- [5] E. Schuster, C. Ziebert, A. Melcher, M. Rohde, and H. J. Seifert, "Thermal behavior and electrochemical heat generation in a commercial 40 ah lithium ion pouch cell," *Journal of Power Sources*, vol. 286, pp. 580–589, 2015.
- [6] T. Cai, A. G. Stefanopoulou, and J. B. Siegel, "Modeling li-ion battery thermal runaway using a three section thermal model," in *Dynamic Systems and Control Conference*, vol. 51906. American Society of Mechanical Engineers, 2018, p. V002T28A003.
- [7] S. Goutam, J.-M. Timmermans, N. Omar, P. V. d. Bossche, and J. Van Mierlo, "Comparative study of surface temperature behavior of commercial li-ion pouch cells of different chemistries and capacities by infrared thermography," *Energies*, vol. 8, no. 8, pp. 8175–8192, 2015.
- [8] B. Wu, Z. Li, and J. Zhang, "Thermal design for the pouch-type large-format lithium-ion batteries: I. thermo-electrical modeling and origins of temperature non-uniformity," *Journal of The Electrochemical Society*, vol. 162, no. 1, p. A181, 2014.
- [9] M. Yazdanpour, P. Taheri, A. Mansouri, and M. Bahrami, "A distributed analytical electro-thermal model for pouch-type lithium-ion batteries," *Journal of The Electrochemical Society*, vol. 161, pp.) A1953–A1963, 09 2014.
- [10] A. Samba, N. Omar, H. Gualous, Y. Firouz, P. Van den Bossche, J. Van Mierlo, and T. I. Boubekeur, "Development of an advanced two-dimensional thermal model for large size lithium-ion pouch cells," *Electrochimica Acta*, vol. 117, pp. 246–254, 2014.
- [11] M. Mastali, E. Foreman, A. Modjtahedi, E. Samadani, A. Amirfazli, S. Farhad, R. A. Fraser, and M. Fowler, "Electrochemical-thermal modeling and experimental validation of commercial graphite/lifepo4 pouch lithium-ion batteries," *International Journal of Thermal Sciences*, vol. 129, pp. 218–230, 2018.
- [12] J. Jaguemont, A. Nikolian, N. Omar, S. Goutam, J. Van Mierlo, and P. Van den Bossche, "Development of a two-dimensional-thermal model of three battery chemistries," *IEEE Transactions on Energy Conversion*, vol. 32, no. 4, pp. 1447–1455, 2017.
- [13] M. Guo and R. E. White, "A distributed thermal model for a li-ion electrode plate pair," *Journal of Power Sources*, vol. 221, pp. 334–344, 2013.
- [14] M. Ghalkhani, F. Bahiraei, G.-A. Nazri, and M. Saif, "Electrochemical—thermal model of pouch-type lithium-ion batteries," *Electrochimica Acta*, vol. 247, pp. 569–587, 2017.
- [15] Y. Xie, X.-j. He, X.-s. Hu, W. Li, Y.-j. Zhang, B. Liu, and Y.-t. Sun, "An improved resistance-based thermal model for a pouch lithium-ion battery considering heat generation of posts," *Applied Thermal Engineering*, vol. 164, p. 114455, 2020.
- [16] S. Goutam, A. Nikolian, J. Jaguemont, J. Smekens, N. Omar, P. V. D. Bossche, and J. Van Mierlo, "Three-dimensional electro-thermal model of li-ion pouch cell: Analysis and comparison of cell design factors and model assumptions," *Applied thermal engineering*, vol. 126, pp. 796–808, 2017.
- [17] X. Lin, H. Fu, H. E. Perez, J. B. Siege, A. G. Stefanopoulou, Y. Ding, and M. P. Castanier, "Parameterization and observability analysis of scalable battery clusters for onboard thermal management," Oil & Gas Science and Technology–Revue d'IFP Energies nouvelles, vol. 68, no. 1, pp. 165–178, 2013.
- [18] X. Lin, H. E. Perez, J. B. Siegel, A. G. Stefanopoulou, Y. Li, R. D. Anderson, Y. Ding, and M. P. Castanier, "Online parameterization of lumped thermal dynamics in cylindrical lithium ion batteries for core temperature estimation and health monitoring," *IEEE Transactions on Control Systems Technology*, vol. 21, no. 5, pp. 1745–1755, 2012.

- [19] D. Zhang, S. Dey, H. E. Perez, and S. J. Moura, "Real-time capacity estimation of lithium-ion batteries utilizing thermal dynamics," *IEEE Transactions on Control Systems Technology*, vol. 28, no. 3, pp. 992– 1000, 2019.
- [20] Y. Kim, J. B. Siegel, and A. G. Stefanopoulou, "A computationally efficient thermal model of cylindrical battery cells for the estimation of radially distributed temperatures," in 2013 American Control Conference. IEEE, 2013, pp. 698–703.
- [21] M. Muratori, N. Ma, M. Canova, and Y. Guezennec, "A model order reduction method for the temperature estimation in a cylindrical li-ion battery cell," in *Dynamic Systems and Control Conference*, vol. 44175, 2010, pp. 633–640.
- [22] R. R. Richardson, P. T. Ireland, and D. A. Howey, "Battery internal temperature estimation by combined impedance and surface temperature measurement," *Journal of Power Sources*, vol. 265, pp. 254–261, 2014.
- [23] S. S. Rath, E. E. Hoedemaekers, and S. S. Wilkins, "Core temperature estimation for a cylindrical cell battery module," in 2020 Fifteenth International Conference on Ecological Vehicles and Renewable Energies (EVER). IEEE, 2020, pp. 1–10.
- [24] X. Lin, H. E. Perez, J. B. Siegel, and A. G. Stefanopoulou, "Robust estimation of battery system temperature distribution under sparse sensing and uncertainty," *IEEE Transactions on Control Systems Technology*, vol. 28, no. 3, pp. 753–765, 2019.
- [25] R. Firoozi, S. Sattarzadeh, and S. Dey, "Cylindrical battery fault detection under extreme fast charging: A physics-based learning approach," in *Unpublished*, 2021. [Online]. Available: https://sites.psu. edu/deylab/files/2020/09/Learning_Based_Battery_Diagnostics.pdf
- [26] X. Lin, A. G. Stefanopoulou, J. B. Siegel, and S. Mohan, "Temperature estimation in a battery string under frugal sensor allocation," in *Dynamic Systems and Control Conference*, vol. 46186. American Society of Mechanical Engineers, 2014, p. V001T19A006.
- [27] V. Lystianingrum, B. Hredzak, and V. G. Agelidis, "Multiple model estimator based detection of abnormal cell overheating in a li-ion battery string with minimum number of temperature sensors," *Journal of Power Sources*, vol. 273, pp. 1171–1181, 2015.
- [28] J. Sun, G. Wei, L. Pei, R. Lu, K. Song, C. Wu, and C. Zhu, "Online internal temperature estimation for lithium-ion batteries based on kalman filter," *Energies*, vol. 8, no. 5, pp. 4400–4415, 2015.
- [29] M. Debert, G. Colin, G. Bloch, and Y. Chamaillard, "An observer looks at the cell temperature in automotive battery packs," *Control Engineering Practice*, vol. 21, no. 8, pp. 1035–1042, 2013.
- [30] N. Tian, H. Fang, and Y. Wang, "3-d temperature field reconstruction for a lithium-ion battery pack: A distributed kalman filtering approach," *IEEE Transactions on Control Systems Technology*, vol. 27, no. 2, pp. 847–854, 2017.
- [31] J. Zhang, J. Huang, Z. Li, B. Wu, Z. Nie, Y. Sun, F. An, and N. Wu, "Comparison and validation of methods for estimating heat generation rate of large-format lithium-ion batteries," *Journal of Thermal Analysis* and Calorimetry, vol. 117, no. 1, pp. 447–461, 2014.
- [32] Y. Xiao, "Model-based virtual thermal sensors for lithium-ion battery in ev applications," *IEEE Transactions on Industrial Electronics*, vol. 62, no. 5, pp. 3112–3122, 2014.
- [33] N. A. Samad, J. B. Siegel, A. G. Stefanopoulou, and A. Knobloch, "Observability analysis for surface sensor location in encased battery cells," in 2015 American Control Conference (ACC). IEEE, 2015, pp. 299–304.
- [34] P. Wolf, S. Moura, and M. Krstic, "On optimizing sensor placement for spatio-temporal temperature estimation in large battery packs," in 2012 IEEE 51st IEEE Conference on Decision and Control (CDC). IEEE, 2012, pp. 973–978.
- [35] R. Caldwell et al., "Hull inspection techniques and strategy-remote inspection developments," in SPE Offshore Europe Conference & Exhibition. Society of Petroleum Engineers, 2017.
- [36] L. Ma and Q. Chen, "Problems and research on underground charging safety of power battery for coal mine robot," in *IOP Conference Series: Earth and Environmental Science*, vol. 651, no. 3. IOP Publishing, 2021, p. 032100.
- [37] G. Zhang, C. E. Shaffer, C.-Y. Wang, and C. D. Rahn, "In-situ measurement of current distribution in a li-ion cell," *Journal of The Electrochemical Society*, vol. 160, no. 4, p. A610, 2013.
- [38] D. Bernardi, E. Pawlikowski, and J. Newman, "A general energy balance for battery systems," *Journal of the electrochemical society*, vol. 132, no. 1, p. 5, 1985.
- [39] N. L. Grubben and K. J. Keesman, "Controllability and observability of 2d thermal flow in bulk storage facilities using sensitivity fields," *International Journal of Control*, vol. 91, no. 7, pp. 1554–1566, 2018.

- [40] A. K. Singh and J. Hahn, "Determining optimal sensor locations for state and parameter estimation for stable nonlinear systems," *Industrial* & engineering chemistry research, vol. 44, no. 15, pp. 5645–5659, 2005.
- [41] V. Lystianingrum, B. Hredzak, and V. G. Agelidis, "Abnormal overheating detectability analysis based on cross gramian for a supercapacitors string," in 2016 IEEE Power and Energy Society General Meeting (PESGM). IEEE, 2016, pp. 1–5.
- [42] M. Serpas, G. Hackebeil, C. Laird, and J. Hahn, "Sensor location for nonlinear dynamic systems via observability analysis and max-det optimization," *Computers & Chemical Engineering*, vol. 48, pp. 105– 112, 2013.
- [43] H. Fang, R. Sharma, and R. Patil, "Optimal sensor and actuator deployment for hvac control system design," in 2014 American Control Conference. IEEE, 2014, pp. 2240–2246.
- [44] S. K. Spurgeon, "Sliding mode observers: a survey," *International Journal of Systems Science*, vol. 39, no. 8, pp. 751–764, 2008.
- [45] S. Dey, B. Ayalew, and P. Pisu, "Nonlinear robust observers for state-of-charge estimation of lithium-ion cells based on a reduced electrochemical model," *IEEE Transactions on Control Systems Technology*, vol. 23, no. 5, pp. 1935–1942, 2015.
- [46] A. Alessandri, "Design of sliding-mode observers and filters for nonlinear dynamic systems," in *Proceedings of the 39th IEEE Conference on Decision and Control (Cat. No. 00CH37187)*, vol. 3. IEEE, 2000, pp. 2593–2598
- [47] H. H. Rosenbrock, "State-space and multivariable theory," 1970.
- [48] P. Moraal and J. Grizzle, "Asymptotic observers for detectable and poorly observable systems," in *Proceedings of 1995 34th IEEE Con*ference on Decision and Control, vol. 1. IEEE, 1995, pp. 108–114.